Eur. Phys. J. D **22**, 17–29 (2003)
DOI: 10.1140/epjd/e2002-00219-7

THE EUROPEAN PHYSICAL JOURNAL D

A novel electron scattering apparatus combining a laser photoelectron source and a triply differentially pumped supersonic beam target: characterization and results for the $He^-(1s\,2s^2)$ resonance

A. Gopalan[1], J. Bömmels[1], S. Götte[1], A. Landwehr[1], K. Franz[1], M.-W. Ruf[1], H. Hotop[1,a], and K. Bartschat[2,b]

[1] Fachbereich Physik, Universität Kaiserslautern, D-67653 Kaiserslautern, Germany
[2] ITAMP, Harvard Smithsonian Center for Astrophysics, Cambridge, MA 02138, USA

Received 23 July 2002
Published online 29 October 2002

Abstract. A novel electron scattering apparatus for high resolution studies of angle-differential elastic and inelastic electron scattering from atoms and molecules in the gas phase is described and its performance characterized. It combines a laser photoelectron source, a triply differentially pumped collimated supersonic beam target (half angle 0.015 rad, background to beam density ratio < 0.01), and several electron multipliers for simultaneous detection of elastically scattered electrons and metastable atoms (or molecules) due to inelastic scattering. In detailed test measurements of the yield for the production of metastable $He^*(2^3S_1)$ atoms around its threshold, the dependence of the overall energy width on various experimental parameters has been investigated. So far a resolution down to 7 meV (FWHM) has been obtained. Under such conditions we have investigated the profile of the $He^-(1s\ 2s^2\ ^2S_{1/2})$ resonance at the scattering angles 22°, 45°, and 90°. From a consistent fit of the measured profiles by resonant scattering theory we determine a new value for the resonance energy ($E_r = 19.365(1)$ eV) and an accurate resonance width ($\Gamma = 11.2(5)$ meV). These results are consistent with the previously recommended values.

PACS. 39.10.+j Atomic and molecular beam sources and techniques – 41.75.Fr Electron and positron beams – 34.80.Bm Elastic scattering of electrons by atoms and molecules – 34.80.Dp Atomic excitation and ionization by electron impact

1 Introduction

Collisions of low-energy electrons with atoms, molecules, and ions are important elementary processes in technical and natural plasmas including gaseous discharges, flames, laser plasmas, high-current switches, arcs and stellar atmospheres. These processes have been investigated for about 100 years, but most notably since the 1960s with the advent of improved vacuum and detector technology and following the discovery of narrow resonances in electron scattering from atoms and molecules [1–8]. Using conventional equipment for electron-energy selection (*e.g.* spherical or cylindrical electrostatic condensors), typical energy widths in low-energy electron scattering experiments involving gaseous targets have been in the range 20–60 meV full width half maximum (FWHM). This resolution is often sufficient to resolve electronic and vibrational levels, but it averages over rotational structure. In a few cases, energy widths around 10 meV (FWHM) have been obtained [9–13]. With specially designed, optimized condensors as monochromators [14], energy widths down to 1 meV have been achieved in electron scattering from adsorbates at surfaces under ultrahigh vacuum conditions [15], but to date such narrow widths have not been demonstrated in scattering from gaseous targets with conventional electron sources.

As a promising alternative to reach very high resolution, near-threshold photoionization of atoms has been exploited as a source for monoenergetic electrons. In a pioneering experiment, Gallagher and coworkers photoionized metastable $Ba^*(^1D_2)$ atoms within the cavity of a cw He–Cd laser at 325 nm, thus providing photoelectrons with a kinetic energy of 17 meV [16–18]. About 10% of these electrons were extracted by a weak electric field and formed into a beam. Subsequently the electrons interacted with atoms and molecules of a singly differentially pumped supersonic target beam in a field-free reaction chamber. At electron beam currents up to 10 pA, elastic scattering from He and Ar atoms as well as from N_2 molecules was reported [17,18]. Effective linewidths of 5–6 meV were observed for the narrow Feshbach resonances in Ar at 11.1 eV

[a] e-mail: `hotop@physik.uni-kl.de`
[b] *Permanent address*: Department of Physics and Astronomy, Drake University, Des Moines, IA 50311, USA.

and N_2 at 11.48 eV [17,18], for which the estimated natural widths are about 3 meV [5,19] and 0.6 meV [20], respectively. Arguments were presented that the energy width of the electron source was $\leq$ 2 meV [17,18]. A non-optimal aspect of this landmark experiment was the rather large angular width of the supersonic beam (about 0.15 rad) and, more importantly, the substantial fraction of thermal background density of the scattering gas in the scattering volume due to insufficient pumping. For helium, the ratio of supersonic beam density to thermal background density in the scattering volume as viewed by the detectors was measured to be about 3 [18]. The presence of the target as a mixture of beam and diffuse thermal gas was accounted for in the analysis of resonances by using superpositions of two contributions with different effective widths [18].

Chutjian and coworkers [21–23] used monochromatized VUV light from a discharge continuum lamp to produce photoelectrons with variable energy at photon bandwidths of typically 6–8 meV and thus studied electron attachment spectra for a broad range of molecules over the energy range 0–160 meV. Field and coworkers used monochromatized synchrotron radiation, first at Daresbury as well as Orsay [24–26] and later at Aarhus [27,28], to photoionize Ar atoms at the Ar($11s'$, $J = 1$) resonance, and thus produced photoelectrons of about 4 meV energy with energy widths around 4 meV [26] (more recently down to 1 meV [27]) at currents around 1 pA. Apart from some initial studies of elastic and inelastic electron scattering from molecules in a supersonic beam [25,26] at scattering angles around 90°, they concentrated on the measurement of total and backward scattering cross-sections from a substantial number of molecules present in a gas cell. In view of the absence of sharp structure in the reported experiments (except for their study of O_2 [29]) it is difficult to infer the actual energy width in these experiments which is limited by the Doppler effect.

Recently, laser photoionization of laser-excited $Ar^*(4p\ ^3D_3)$ [30–33] as well as $Na^*(3p)$ [34] and $K^*(4p)$ [35–37] atoms has been exploited for laser photoelectron attachment (LPA) experiments at current levels between 1 and 200 pA. Ionizing with a single-mode laser and thus producing currents around 0.03 pA, Schramm *et al.* [32] have demonstrated energy widths as low as 20 μeV at collision energies down 20 μeV. At currents above 10 pA, the effects of photoion space charge are expected to increasingly influence the achievable resolution [38].

With the aim to investigate low-energy electron scattering processes involving gaseous targets at energy widths down to 1 meV resolution, we have constructed a new apparatus which is based on the experience in previous work and combines the following aspects:

(a) production of a collimated electron beam with currents up to 100 pA and energy widths of a few meV, using a laser photoelectron source;
(b) a well-collimated and dense supersonic beam target, directed perpendicularly to the electron beam, to reduce Doppler broadening and background scattering to negligible levels;
(c) parallel detection of (elastically) scattered electrons at several angles;
(d) simultaneous detection of long-lived excited atoms (*e.g.* metastable He^* atoms), produced by inelastic electron scattering, allowing for a precise calibration of the electron energy scale by determining the excitation threshold.

In Section 2 we describe the new apparatus in some detail. Following a brief summary of the theoretical description of the investigated processes (Sect. 3), we demonstrate the present performance of the new setup, as characterized by measurements involving elastic and inelastic scattering from helium atoms (Sects. 4.1 and 4.2). Measuring jointly the cross-section for elastic scattering at the three angles 22°, 45°, and 90° over the range 19.26–19.46 eV and the yield for metastable $He^*(2^3S_1)$ atoms around threshold at energy widths of 7–8 meV, we have determined accurate values for the resonance width Γ and the resonance energy E_r of the $He^-(1s\ 2s^2\ ^2S_{1/2})$ resonance at 19.365 eV (Sect. 4.3). We conclude with a summary and a brief discussion of future perspectives (Sect. 5).

2 Experimental apparatus

2.1 Vacuum system, target beam, and potassium atom beam

A vertical cut through the apparatus is shown in Figure 1. It consists of five separately pumped chambers. The nozzle chamber NC, the intermediate chamber IC, and the dump chamber DC serve to create an intense, well collimated Campargue-type [39] supersonic beam target of atoms or molecules in the reaction volume, located in the main chamber MC. This setup and its performance have been described before in detail [40]. In the present work, a sonic nozzle (diameter 0.2 mm) in conjunction with a conical skimmer (Beam Dynamics, Mod. 31.8, diameter 0.7 mm, Fig. 8a in [40]) between NC and IC and a conical skimmer (diameter 1.93 mm) between IC and MC have been used. In the target plane, located about 160 mm above the nozzle orifice, the collimated beam has a diameter of 4.3 mm. For helium, the gas of interest for the measurements addressed in this paper, target densities were about 4×10^{12} cm^{-3} at stagnation pressures of $p_0 = 5.5$ bar (nozzle temperature $T_0 = 300$ K); the quoted density is the average of the values estimated from *in situ* electron impact ionization and from the pressure rise in DC [40]. Under these conditions the background helium density (due to backstreaming from DC, intra-beam scattering and scattering from the two skimmers) is at least 100 times lower. The base pressure in MC (target beam off) amounted to about 1×10^{-7} mbar.

The oven chamber OC actually consists of two subchambers which are evacuated jointly by one pump. For maintenance purposes involving the potassium oven, this chamber can be separated from MC by a slide valve. Below this valve, a combination of two aluminum tubes and

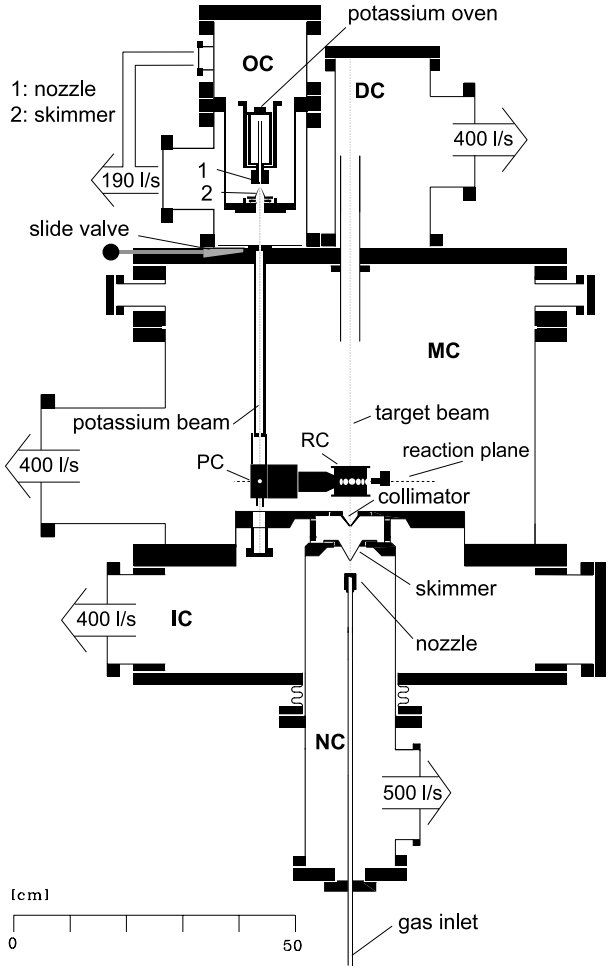

Fig. 1. Experimental setup (vertical cut). NC: nozzle chamber, IC: intermediate chamber, MC: main chamber, DC: dump chamber, OC: oven chamber, PC: photoionization chamber, RC: reaction chamber.

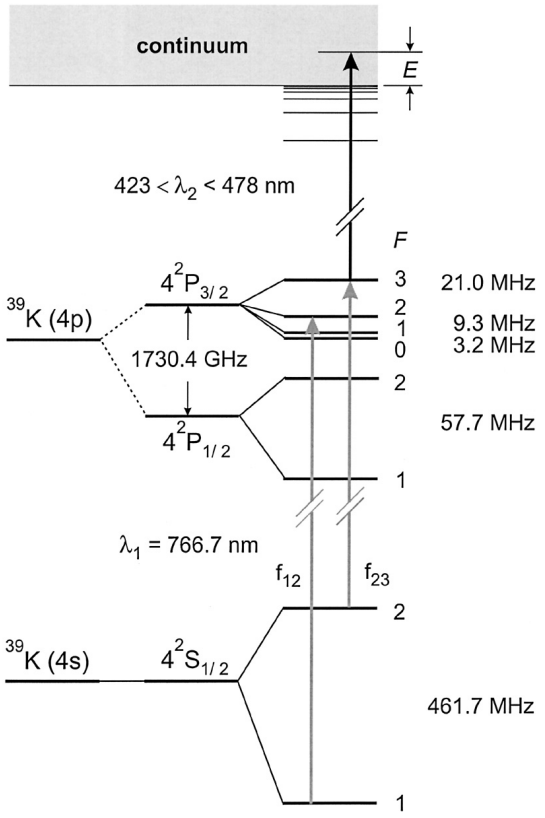

Fig. 2. Excitation scheme for photoelectron production (see text).

a PTFE insulated plate (the latter being fixed to the photoionization chamber PC) provide an essentially gas-tight connection between OC and PC, thus preventing the potassium vapour from spreading in MC. After passing through PC, the potassium atoms are dumped into an extension tube of MC. The potassium beam is generated in a two-stage oven, operated in the effusive regime. Typical temperatures are $T_R = 532$ K for the reservoir and $T_N = 597$ K for the nozzle (diameter $D_N = 1$ mm). The beam is collimated by a conical, heated skimmer (hole diameter 1.5 mm, temperature $T_S = 593$ K, distance from nozzle about 15 mm). Under these conditions the potassium density in the photoionization region (distance from nozzle 530 mm) amounts to about 1.7×10^8 cm^{-3}.

2.2 Laser photoelectron source, electron beam formation and product detection

The photoelectron production is based on resonant two-step photoionization of potassium atoms *via* the $K^*(4p_{3/2})$ level [36,37], see Figure 2. Both hyperfine components of ground state $^{39}K(4s,\ F = 1, 2)$ atoms in the collimated potassium beam (size 1×3 mm) are transversely excited to the $^{39}K^*(4p_{3/2},\ F = 2, 3)$ states by the first sidebands of the electro-optically modulated (frequency 220.35 MHz) output of a single-mode cw titanium: sapphire laser ($\lambda_1 = 766.7$ nm); the latter is long-term stabilized to the atomic transition by crossover saturation spectroscopy in an auxiliary potassium vapour cell [41]. Part of the excited state population is photoionized by interaction with the intracavity field of a multimode tunable dye laser (energy width 0.15 meV, power up to 7 W), operated in the blue spectral region (dye Stilbene 3). The photoionization scheme in Figure 2 has previously been applied to electron attachment experiments involving molecules and molecular clusters at meV energy width [35,36,42]; in these former studies, electrons were generated with variable energies (0–200 meV) by continuous tuning of the wavelength of the ionization laser. In the present work electrons are created near threshold ($\lambda_2 = 455$ nm, energy below 1 meV). Using low-loss fused silica windows and cylindrical lenses (V-type AR coating at 455 nm, measured transmission at 767 nm about 95%) within the cavity, the ionization laser is focussed to a ribbon of about 1 mm height and 0.1 mm width in the electron extraction direction. The infrared laser is superimposed collinearly with the ionization laser, entering through the terminating mirror (transmission 0.94(1)% at 455 nm and about 98% at 767 nm) of the latter. The infrared laser is thus

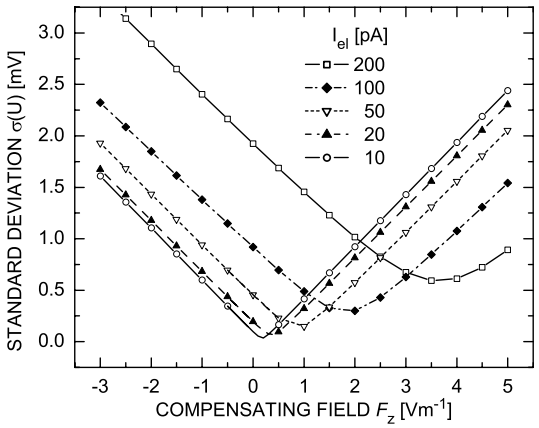

Fig. 3. Results of Monte Carlo simulations for the standard deviation $\sigma(U)$ of the potential distribution $f(U)$ in the electron source volume due to the photoion space charge and the superimposed compensation field F_z along the potassium beam for different values of the photoelectron current $I_{\rm el}$ and of the compensation field F_z.

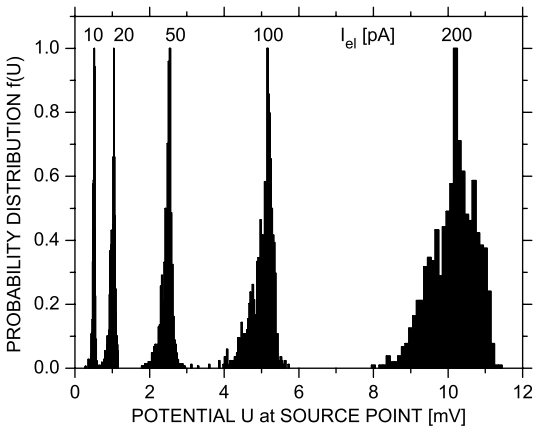

Fig. 4. Results of Monte Carlo simulations for the potential distributions $f(U)$ in the electron source volume with optimized compensation field F_z.

also brought to a cylindrical focus with extensions somewhat wider than those of the ionization laser. Test experiments showed that the photoelectron current was independent of the infrared laser power at levels above 10 mW; in the scattering experiments, the power of the infrared laser amounted to typically 80 mW. The photoelectron current was found to vary linearly with intracavity power (about 18 pA per Watt of standing wave power of the blue laser). In order to characterize the influence of the photoion-induced space charge on the effective energy width of the electron beam, Monte Carlo simulations were carried out in a way described previously [38]. In Figure 3 we present the current-dependent standard deviations of the potential distribution in the electron source volume which are due to the effects of photoion space charge and additional homogeneous electric fields F_z applied along the direction of the potassium beam. As seen from the results in Figure 3, this field F_z allows to minimize the potential variation in the electron source volume which is associated with the rise of the photoion space charge potential along the vertical z-direction. This possibility has been exploited by our group in electron attachment studies involving the potassium photoelectron source [38]. Figure 4 shows the potential distributions in the photoelectron source volume which are obtained for currents in the range 10–200 pA when an optimized field F_z has been applied. Under these conditions we expect that at electron currents up to 50 pA energy widths below 2 meV should be attainable.

The photoelectrons are accelerated by a weak electric field (typically about 10 V/m) and brought to the energy of interest by an electron optical system (see Fig. 5) which focusses the electron beam onto the perpendicular target beam. Geometric and electron optical considerations (including the divergence of the target beam, half angle 0.015 rad) indicate that the deviations from perpendicular impact are at most ±0.03 rad. Up to five electron detectors, equipped with a retarding electric field and a channel electron multiplier (Sjuts Mod. KBL 10 RS, diameter of entrance cone 10 mm), serve to measure simultaneously the intensity of elastically scattered electrons at several angles of choice, as illustrated in Figure 6. A rectangular entrance aperture (4 mm wide, 6 mm high, located 32.5 mm from the scattering center) limits the angular acceptance range of the electron detectors to ±3.5°. It is followed by a circular lens element (diameter 10.6 mm, length 4 mm) and a pair of grids (diameter 10.6 mm) which form a retarding field, rejecting inelastically scattered electrons. An additional electron multiplier (Sjuts, Mod. KBL 20 RS, diameter of entrance cone 20 mm), mounted at the kinematically adequate position, samples long-lived excited ("metastable") atoms due to inelastic electron scattering (see Fig. 5). Ground state helium atoms (flow velocity $u = [5k_{\rm B}T_0/(2m_{\rm He})]^{1/2} = 1\,775$ m/s at $T_0 = 300$ K), which are excited to the metastable $\mathrm{He}^*(2^3\mathrm{S}_1)$ level by a perpendicular monoenergetic electron beam at threshold (transition energy $E_{\rm T} = 19.8196$ eV, taken from [43] with the conversion $1.239\,842\,44(37) \times 10^{-4}$ eV/cm^{-1} [44]), are deflected by a (lab) angle of 11.5°. At an electron energy of 1.2 eV above threshold, for example, the deflection angles are spread over the range 9.1−14.7°, which essentially corresponds to the maximum acceptance angle of the channel electron multiplier.

The detection of metastable $\mathrm{He}^*(2^3\mathrm{S}_1)$ atoms serves an important purpose: based on the well-known threshold energy and the accurate theoretical cross-section for the production of $\mathrm{He}^*(2^3\mathrm{S}_1)$ atoms [45,46], one can precisely determine – by comparing the measured yield for metastable atom production with that obtained by convolution of the theoretical cross-section with an appropriate resolution function – both the absolute electron energy scale *and* the effective energy width of the scattering experiment. Note that small differences exist between the laboratory electron energy $E = m_{\rm e}\mathbf{v}_{\rm e}^2/2$ and the relative collision energy $E_{\rm rel}$ in the center-of-mass frame which is given by

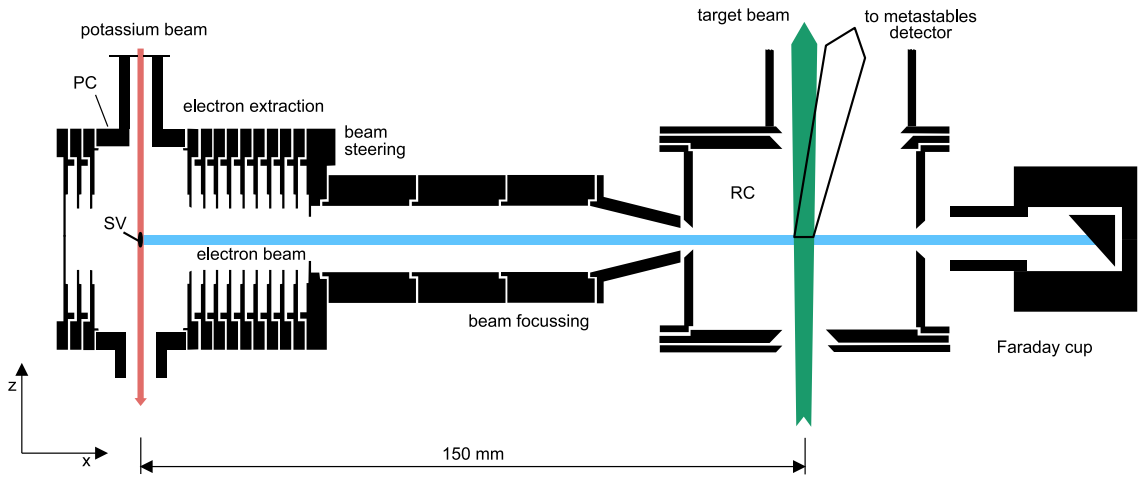

Fig. 5. Photoelectron source, electron optics, reaction chamber (RC) and Faraday cup, as seen in a vertical cut (PC: photoionization chamber, SV: electron source volume). The two laser beams intersect the potassium atom beam perpendicularly to the drawing plane (*i.e.* along the y-direction).

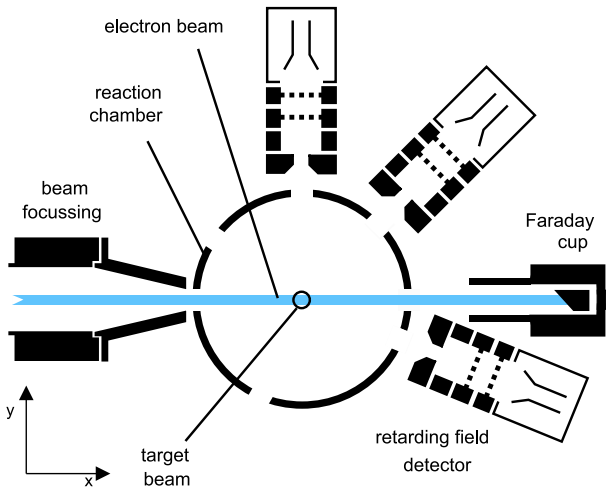

Fig. 6. View of experimental setup in the (horizontal) reaction plane.

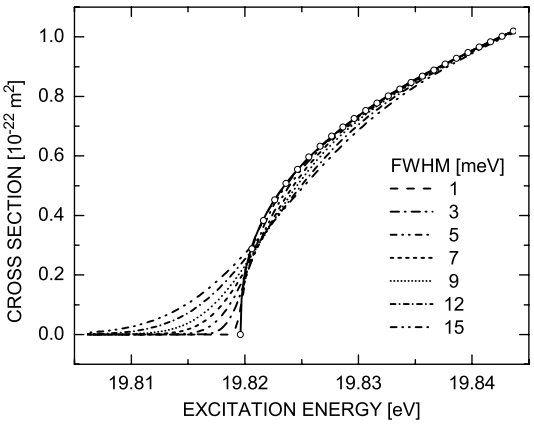

Fig. 7. Threshold region of the theoretical cross-section for electron impact excitation of $He^*(2^3S_1)$ atoms (open circles, interpolated by full curve) and broadening induced by Gaussian resolution functions of widths (FWHM) between 1 meV and 15 meV.

($E_T = m_T \mathbf{v}_T^2/2 =$ kinetic energy of target particles)

$$E_{rel} = (1/2)[m_e m_T/(m_e + m_T)](\mathbf{v}_e - \mathbf{v}_T)^2. \quad (1)$$

This is very well approximated by

$$E_{rel} \approx E - (m_e/m_T)E - 2(m_e E E_T/m_T)^{1/2}\cos\theta. \quad (2)$$

The second term in (2) is the recoil energy E_R transferred to the target by the incoming electron while the third term represents the energy shift E_D due to the first-order Doppler effect. Near the threshold for $He^*(2^3S_1)$ excitation ($E \approx 19.82$ eV) the recoil energy amounts to $E_R = 2.72$ meV and the Doppler shift to $E_D = 26.57\ \text{meV} \times \cos\theta$, *i.e.* for deviations of θ from 90° below 0.03 rad (about 1.7°) $|E_D| \leq 0.797$ meV. When comparing the energy for the threshold of $He^*(2^3S_1)$ excitation with that for the position of the $He^-(^2S_{1/2})$ resonance ($E \approx 19.365$ eV, $E_R = 2.65$ meV, $|E_D| \leq 0.779$ meV), the energy separations between the two respective electron energies in the laboratory and the center-of-mass frame differ mainly by the non-identical recoil energies.

In Figure 7 we present the theoretical cross-section for the production of metastable $He^*(2^3S_1)$ atoms over the energy range 19.80−19.85 eV (full curve); near threshold it is well described by the analytical function $f(E) = f_0(E - E_T)^{0.391}$ with $f_0 = 4.3786 \times 10^{-22}$ m^2 and E in eV. We note that an exponent of 0.5 is expected according to Wigner's law [47] (close to threshold the outgoing inelastically scattered electron should be predominantly s-wave), but in view of the high polarizability of $He^*(2^3S_1)$ atoms ($315.63a_0^3$ [48]) the Wigner law is expected to hold over only a very narrow energy range above threshold (see, *e.g.*, [49]). In Figure 7 we also show effective cross-sections obtained by convolution of the theoretical

cross-section with a Gaussian resolution function of the indicated widths (FWHM between 1 and 15 meV).

2.3 Voltage sources and data acquisition

Since the electron energy width in the experiment is directly influenced by the stability and noise figures of the voltage sources used to supply the potentials to the electron optical components (especially of the source providing the voltage between the photoionization and the reaction chamber), highly stable, low-noise computerized voltage sources had to be developed. Eight serial input, 16-bit high precision digital-to-analog converters (Burr Brown DAC 714; noise, differential and integral nonlinearity figures below 1 least-significant-bit) were combined, together with signal conditioning and interface circuitry, into voltage supply systems which can be directly attached to d-sub 9 pin vacuum feedthroughs mounted on DN40-CF vacuum flanges, eliminating the need for shielded cables to transport the potentials from the source to the electrically and magnetically shielded vacuum system. Five of these systems (providing a total of 40 independently controllable voltages) are connected to a host computer (Pentium III, 800 MHz, running Linux 2.2), using an optically coupled two-wire serial bus running a multi-master communication protocol with error-detection at a bit-rate of 622 kbits/s. Additional data-acquisition hardware such as a fast six-channel counter is attached to the same bus system. The host computer is running a graphically programmable, versatile data acquisition system which controls the measurement and drives the data acquisition. The complete set of parameters can be easily stored and restored, and semi-automatic optimization procedures can readily be implemented using this system. Ground-loops and shield-loops have been carefully avoided in the design of the system, yielding overall noise and ripple figures below 1 mV.

2.4 Shielding of electric and magnetic fields

Electric stray fields in the photoionization and scattering regions are to be carefully avoided, since the resulting potential drops over the interaction regions are directly translated to a corresponding broadening of the effective electron energy width. Common design rules have been followed to minimize such fields: no line-of-sight exists from the critical regions to any insulating materials such as standoffs, spacers and insulated wires, and shielding extension tubes are attached to all outer orifices of the electron optical system. The vacuum enclosure effectively shields the experiment from external electric fields. An additional double magnetic shielding made of mu metal (1.5 mm thick) reduces the residual magnetic field components in the chamber to values below 1 mG in the horizontal plane and well below 6 mG in the vertical direction. It may be noted that in the present setup static magnetic fields have no influence on the effective electron energy width. *In situ* measurements of ac electric fields (ripple) on the electrodes are difficult to perform at the (sub)meV level. As discussed in Section 2.3 the individual potentials provided to the cables which connect to the electrodes have measured ripple below 1 meV. In order to rule out significant 50 Hz noise on the voltage which defines the electron collision energy (apart from contact and surface potential differences) special test measurements were carried out (see Sect. 4.1).

3 Theoretical description

The numerical calculations performed for the present work are based upon the R-matrix with pseudo-states (RMPS) approach described by Bartschat *et al.* [45] and Bartschat [46], to be referred to as RMPS1 and RMPS2 below. Briefly, these are close-coupling models including the lowest five (RMPS1) or eleven (RMPS2) physical target states of He together with 36 (RMPS1) or 35 (RMPS2) pseudo-states to represent the effect of the infinite number of discrete states as well as the ionization continuum on the results for transitions between the physical states. Due to the short range of the pseudo-states (essentially covering the radial region around the physical states of interest), these models are expected to be very accurate for the comparisons of interest in the current experimental investigation.

Besides accounting for the coupling between the many physical and pseudo-states, a major strength of the above model is the very accurate (compared to other coupled-channel collision calculations) structure description of the discrete target states. Note that the need for treating both the N-electron target and the $(N + 1)$-electron collision problem simultaneously makes it practically impossible to achieve the same accuracy as in structure-only calculations. Hence, it is important to discuss possible effects caused by the remaining deficiencies in the structure model. The biggest such effect is usually in the ground-state energy, which is not low enough even with the multi-configuration expansion used for the present work. On the other hand, the $(n = 2)$ excited states are very well described (see Tab. 1 of [45]).

In the RMPS1 calculation [45], it was therefore decided to use the theoretical threshold energies instead of making adjustments to reflect the experimental energy splittings. The major advantage of not adjusting the target thresholds is the fact that this keeps the maximum consistency between the N-electron and the $(N+1)$-electron descriptions. However, resonance positions, such as that of the $(1s\ 2s^2)^2\mathrm{S}_{1/2}$ resonance, should then be given in terms of their binding energy with respect to the corresponding target threshold (here $2^3\mathrm{S}_1$) rather than in terms of an absolute energy with respect to the ground state. To compare directly with experiment, the energy scale can then effectively be adjusted afterwards by counting backwards from the experimental $2^3\mathrm{S}_1$ threshold. In the RMPS1 calculation, this adjustment is 104.5 meV by which the ground-state energy effectively has to be moved down. On the experimental scale, the position and width of the $(1s\ 2s^2)^2\mathrm{S}_{1/2}$ resonance in the above model are then $E_r = 19.366$ eV and $\Gamma = 10.7$ meV, respectively [45].

Table 1. Phases δ_L and derivatives $d\delta_L/dE$ of phase function for $L = 0$, 1, 2 partial waves in potential scattering from helium atoms at the energy of the $He^-(1s\ 2s^2\ ^2S_{1/2})$ resonance ($E_r = 19.365$ eV).

Reference	δ_0 [rad]	$d\delta_0/dE$ [rad/eV]	δ_1 [rad]	$d\delta_1/dE$ [rad/eV]	δ_2 [rad]	$d\delta_2/dE$ [rad/eV]
Experiment						
Andrick, Bitsch [51]	1.81(9)[a]		0.325(40)[a]			
Williams [52]	1.794(25)[b]	−0.016	0.312(4)[b]	+0.004	0.058[b]	+0.004
Kennerly *et al.* [18]	1.813(17)		0.307(14)			
Dubé *et al.* [55]	1.778		0.317		0.076	
Theory						
Nesbet [53]	1.796[c]		0.319[c]		0.059[c]	
Bartschat *et al.* [45]	1.7995[b]	−0.0123	0.3162	+0.0094	0.0586	+0.0024

[a] Values taken from Table I in [55]. [b] Interpolated values. [c] Extrapolated values, taken from Table I in [55].

The RMPS2 model [46], on the other hand, is somewhat more suitable for direct comparison with experiment for the excitation processes, since the theoretical thresholds were adjusted to coincide with the experimental values. Overall, the agreement between the predictions from RMPS1 and RMPS2 is extremely good, with no more than a 0.5% difference in the non-resonant background. For very sharp structures, within a few meV of an excitation threshold, there may be bigger differences in the predictions, but we have checked that the qualitative behaviour of all curves shown here is the same. Finally, for the comparisons shown in the present paper, we performed calculations in steps of 0.5 meV for the energy range of interest. Partial-wave contributions up to $L = 6$ were sufficient to achieve convergence for all parameters of interest.

Before the present RMPS calculations became available, we used the following approach to model the experimental data. The theoretical expression describing the differential cross-section for elastic scattering $d\sigma/d\Omega = |f(\theta)|^2$ involves the usual partial wave sum for the scattering amplitude $f(\theta)$ [50]

$$f(\theta) = 1/(2ik)\sum_{L=0}^{\infty}(2L+1)[\exp(2i\delta_L) - 1]P_L(\cos\theta). \quad (3)$$

Here, k is the momentum of the electron, δ_L the phase shift for elastic scattering, and $P_L(\cos\theta)$ the Legendre polynomial. For elastic electron scattering from helium atoms at energies around the $He^-(1s\ 2s^2\ ^2S_{1/2})$ resonance (19.365 eV), partial waves higher than $L_c = 2$ do not penetrate to the inner part of the atom [51–53] and so only feel the long-range part of the electron-atom interaction which is the dipole polarization potential $V_{pol} = -\alpha(2r^4)^{-1}$ (α = atomic polarizability, $\alpha(He) = 1.384a_0^3$, a_0 = Bohr radius [48]). As shown by Thompson [54] the contribution to the scattering amplitude due to partial waves $L > L_c$ can to a good approximation be represented by the expression

$$f_B(L > L_c) = (\pi\alpha k/a_0)\big[(1/3) - (1/2)\sin(\theta/2) - \sum_{n=1}^{L_c}[(2n+3)(2n-1)]^{-1}P_n(\cos\theta)\big]. \quad (4)$$

The resonance in the $L = 0$ channel is taken into account by using the s-wave phase shift in the following form:

$$\delta_{L=0} = \delta_{bg} + \delta_r(E) = \delta_{bg} - \mathrm{arccot}[(E - E_r)/(\Gamma/2)] \quad (5)$$

where δ_{bg} represents the background (*i.e.* non-resonant) part of the $L = 0$ phase shift which is nearly independent of energy over the range of the narrow resonance (energy width Γ, resonance energy E_r) and $\delta_r(E)$ is the resonant part of the phase shift which rises from 0 to π when the electron energy increases from lower to higher energies through the resonance energy. Using equations (3–5) and the energy independent (background) phase shifts for $L = 0, 1, 2$ listed in Table 1, differential cross-sections have been calculated which were fitted to the measured resonance profiles with Γ and E_r as adjustable parameters.

4 Results and discussion

4.1 Test measurements

The apparatus has been characterized in series of detailed test measurements involving elastic and inelastic scattering from helium atoms in order to study the influence of the experimental parameters (*i.e.* the electron current and the potentials on the electrodes of the photoionization and the scattering chamber) on the effective energy width in the scattering experiments. Under optimum conditions energy widths ΔE (FWHM) down to 7 meV have been achieved so far, as determined from fits to the $He^*(2^3S_1)$ excitation function near threshold. An example of such a threshold scan and the corresponding fit ($\Delta E = 7.8(5)$ meV) is shown in Figure 8. In agreement with expectations, based on the 100 μm width of the ionization laser in the electron extraction direction and with measurements at electric extraction fields F_{ex} over the range 10–180 V/m, the corresponding potential gradient across the ionization volume leads to a broadening of $\Delta E_{ex}/F_{ex} = 0.1$ meV/(V/m), *i.e.* to an expected width of 1 meV at the typically applied extraction field of 10 V/m. Application of a suitable potential difference to

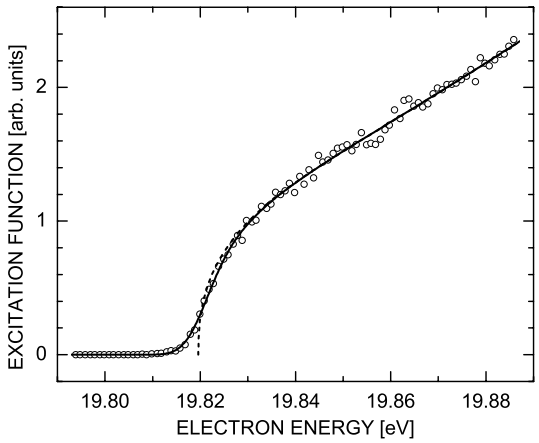

Fig. 8. Threshold measurement of the yield for electron impact excitation of $He^*(2^3S_1)$ atoms (open circles). The full curve is a fit to the experimental data, resulting from a convolution of the theoretical cross-section (broken curve) with a Gaussian resolution function of 7.8(5) meV FWHM.

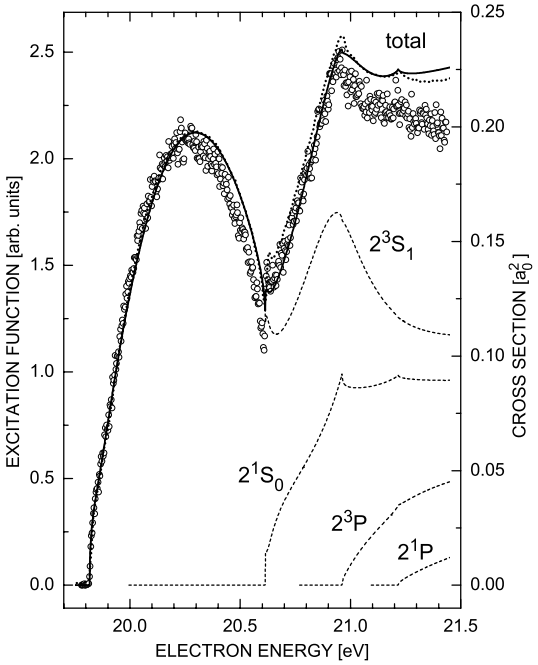

Fig. 9. Excitation function for the production of metastable $He^*(2^3S_1, 2^1S_0)$ atoms in the energy range 19.8–21.5 eV. Full curve: RMPS theory (assuming relative detection efficiencies for 2^3S_1 and 2^1S_0 atoms of 1 and 0.8, respectively); dotted curve: experiment of the Manchester group [56,57]; open circles: present result (channel width 3.0 meV). Dashed curves: absolute partial theoretical excitation cross-sections.

the electrodes along the potassium beam served to minimize the influence of the potential gradient in the ionization volume arising in this direction, as discussed in Section 2.2. Along the direction of the lasers, a potential difference close to zero was found to be optimal. Separate potentials could be applied to the top and bottom plates of the cylindrical reaction chamber and to the cylinder itself; it turned out that optimal conditions were obtained by application of a small voltage (about 0.05 V) along the direction of the target beam. As a modified version of the reaction chamber, implemented after the data of this paper were taken, we now use a cylinder with four segments to which separate potentials can be applied, thus allowing for compensation of residual dc electric fields in the two orthogonal horizontal directions including that of the electron beam. This change did not result in a further reduction of the effective energy width.

To test for possible energy broadening caused by ground loops at the power line frequency of 50 Hz, the width and position of the $He^*(2^3S_1)$ threshold have been measured in a phase-sensitive way using a phase-detector on three different phases of the line voltage and a gated counter to measure the signal in the positive and negative portion of the power line sine-wave. No measurable differences in energy position and broadening have been found, ruling out 50 Hz ground loops as a possible cause for energy broadening above 1 meV.

4.2 Excitation function for the production of metastable $He^*(2^3S_1, 2^1S_0)$ atoms

In Figure 9 we compare the yield for the production of metastable $He^*(2^3S_1, 2^1S_0)$ atoms, measured over the energy range 19.7–21.5 eV (open circles), with an experimental excitation function obtained by the Manchester group [56,57] (dotted curve) at an energy width slightly below 20 meV and with the theoretical prediction (full curve) [46]. The experimental and theoretical results are normalized to the same value at $E = 20.25$ eV. Note that apart from the two metastable levels, short-lived states are formed at energies above 20.9 eV (2^3P) and 21.2 eV (2^1P). The 2^3P_J states decay to the 2^3S_1 level, thus their contribution was added to the 2^3S cross-section. The 2^1P level predominantly decays to the ground state (only 1 in 1 000 decays leads to the 2^1S_0 level [58]), and its contribution to the metastable flux is negligible in the energy range of interest. Note that the fraction of 58.4 nm photons due to the $2^1P \rightarrow 1^1S_0$ optical decay which hit the metastable atom detector is small because of angular discrimination. In constructing the theoretical curve for comparison with the experimental data one has to choose appropriate weighting factors for the two metastable levels according to their detection efficiencies (see also [56]). To first order, one may assume that the probability for electron ejection at the gas-covered surface of the metastable atom detector is identical for $He^*(2^3S_1)$ and $He^*(2^1S_0)$ atoms, but differences of up to about 30% cannot be ruled out (see [56,59] and references herein). In constructing the theoretical excitation functions in Figures 9 and 10, we use relative detection efficiencies for 2^3S_1 and 2^1S_0 atoms of 1 and 0.8, respectively. Close agreement between the theoretical $He^*(2^3S_1)$ yield and that measured by Brunt *et al.* [56,57] is observed while the shape obtained in the present work is slightly different, but still in good agreement with the other results, especially over the range

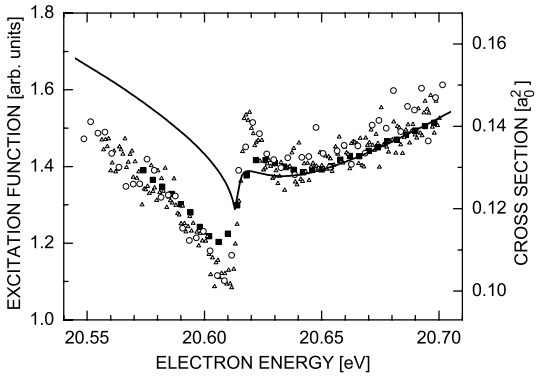

Fig. 10. Shape of the excitation function for the production of metastable $He^*(2^3S_1, 2^1S_0)$ atoms in the energy range 20.55–20.70 eV. Full curve: RMPS theory (assuming relative detection efficiencies for 2^3S_1 and 2^1S_0 atoms of 1 and 0.8, respectively); open circles: present experiment (channel width 3 meV), open triangles: present experiment (channel width 0.75 meV), full squares: experiment of Brunt *et al.* [56].

19.8–20.4 eV. We note that at energies of about 1 eV and more above the 2^3S_1 threshold our data may be affected by a decrease in the overall detection efficiency for 2^3S_1 atoms due to their rising angular spread associated with the momentum transfer from the exciting electron; it is also possible that the detection efficiency of the channel electron multiplier is not homogeneous over the full range of the entrance cone. These effects may also be present in the data of Brunt *et al.* (see discussion in [56]), but possibly to a lesser extent because these authors used an effusive, uncollimated atomic beam.

In the region of the $He^*(2^1S_0)$ threshold, our data exhibit the most prominent minimum and the strongest rise in the excitation function. The slope of this rise appears to be limited by the experimental resolution. We note that in view of the high polarizability of the $He^*(2^1S_0)$ state ($801.1a_0^3$ as compared to $315.63a_0^3$ for the 2^3S_1 level [48]) it is not surprising – as seen in the theoretically calculated threshold rises for these two levels – that the 2^1S_0 cross-section is distinctly steeper at threshold than that for the 2^3S_1 level (see Fig. 9). In Figure 10, we compare the unconvoluted theoretical excitation cross-section (full line) with three different sets of experimental results over the narrow energy range 20.55–20.70 eV: the open circles are taken from our data in Figure 9 (channel width 3.0 meV), the open triangles were obtained in a different run over limited energy ranges around the 2^3S_1 and the 2^1S_0 thresholds (channel width 0.75 meV), and the full squares are data of the Manchester group, obtained around the 2^1S_0 onset with an energy width of about 13 meV (see Fig. 4 in [56]) and here normalized to our data at the midpoint of the rise at the 2^1S_0 threshold. Due to improved resolution (width around 8.5 meV), our data exhibit – apart from the deep minimum and the steep rise at the 2^1S_0 threshold – a sharp maximum just above the 2^1S_0 onset, a feature only weakly present in the theoretical results and in the Manchester data. Note that a different choice for the relative efficiencies in detecting the 2^3S_1 and the 2^1S_0 metastable atoms would not change the theoretical curve much; in particular, it would not produce a sharp maximum in the excitation function. We attribute the narrow peak in our data to the presence of a very sharp threshold *peak* very close to the 2^1S_0 onset. The existence of such a peak, associated with a virtual resonance state of $^2S_{1/2}$ symmetry, has been suggested for some time [60–62]. Perhaps the clearest previous experimental evidence for a sharp threshold peak in the 2^1S_0 cross-section was presented by Allan [63] who reported angle-differential (20−120°) excitation functions for all the $n = 2$ states in He for electron impact energies from threshold to about 24 eV at an energy width of 16–20 meV. By measurements over the full angular range from 0° to 180° [63,64], Allan also demonstrated that the excitation function for 2^3S_1 atoms does *not* show a clear peak just above the 2^1S_0 onset.

4.3 The $He^-(1s\ 2s^2\ ^2S_{1/2})$ resonance revisited

Measuring jointly the cross-section for elastic scattering at the three angles 22°, 45°, and 90° over the range 19.26–19.46 eV (Fig. 11) and the yield for metastable $He^*(2^3S_1)$ atoms around its threshold (Fig. 8) at energy widths around 7.5 meV, we have determined accurate values for the resonance width Γ and the resonance energy E_r of the $He^-(1s\ 2s^2\ ^2S_{1/2})$ resonance at 19.365 eV by fitting theoretical cross-sections (see Sect. 3) with adjustable values for Γ, E_r and the FWHM of the experimental energy resolution function (assumed to be Gaussian) to the experimental data. Note that the electron detection efficiency at the different angles was found to be non-equal which we attribute to non-identical responses of the channel electron multipliers as well as to somewhat different action of the retarding field preceding each multiplier (needed to reject electrons with improper energy which are due, *e.g.*, to scattering from surfaces). As can be seen by comparison of the measured counting rate outside the resonance (left ordinate scale in Fig. 11) with the respective size of the calculated differential cross-section, the relative detection efficiencies at $\theta = 22°$, 45°, and 90° were 0.65, 1.0, and 0.55. From the fits to the experimental spectra, we obtained the values $\Gamma = 11.2(5)$ meV and $E_r = 19.365(1)$ eV consistently for the measurements at the three angles, using the same Gaussian resolution function with FWHM = 7.4(5) meV which is in good agreement with the energy width of 7.8(5) meV, obtained from the fit to the threshold of $He^*(2^3S_1)$ excitation (see Fig. 8). The dashed lines in the spectra of Figure 11 present the differential cross-sections calculated with the RMPS theory ($\Gamma = 10.7$ meV, $E_r = 19.366$ eV) and convoluted with the experimental resolution function (Gaussian, 7.4 meV FWHM). Very good overall agreement with the experimental data is observed which demonstrates – as also observed in the comparison for $He^*(2^3S_1)$ excitation (see Fig. 9) – the reliability of the RMPS method [45] when applied to elastic and inelastic electron scattering from helium atoms. Close comparison of the theoretical and experimental resonance shapes reveals that the theoretical

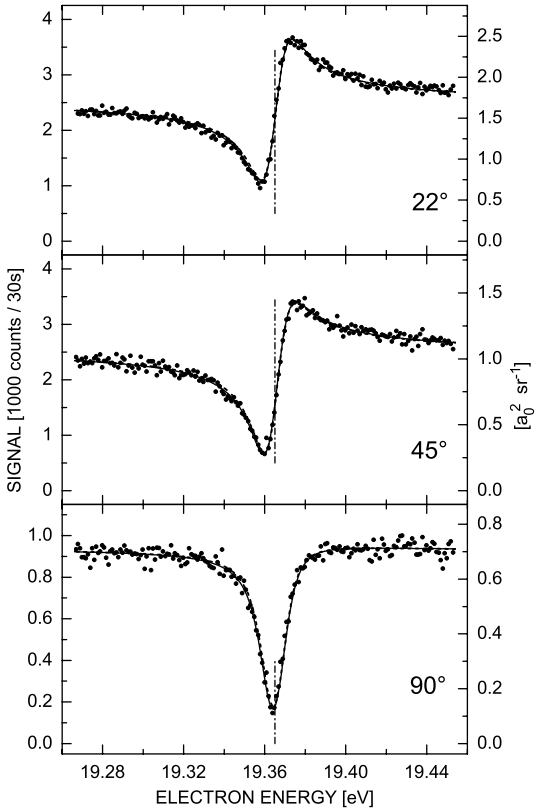

Fig. 11. Resonance profiles for the $He^-(1s\ 2s^2\ ^2S_{1/2})$ resonance, as observed at scattering angles of 22°, 45° and 90°. Full circles: experimental data points (background subtracted); full curves: fitted resonance profiles involving (consistently at the three angles) a Gaussian resolution function with 7.4(5) meV FWHM and a resonance width $\Gamma = 11.2(5)$ meV; dashed curves: results of RMPS theory, convoluted with a Gaussian resolution function with FWHM of 7.4 meV; vertical dash-dotted lines: resonance position $E_r = 19.365$ eV.

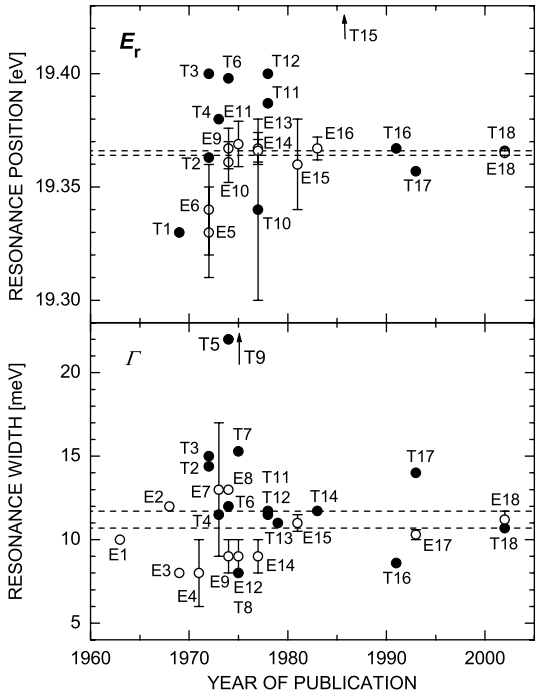

Fig. 12. Summary of previous and present experimental (open circles) and theoretical (full circles) results for the energy position E_r and the width Γ of the $He^-(1s\ 2s^2\ ^2S_{1/2})$ resonance. See Table 2 for references.

width is a little lower than the experimental value as reflected by the numerical values. The error estimate, assigned to our experimental width, reflects in a conservative way the scatter of fitted widths when different sets of scattering phases (see Tab. 1) and appropriate experimental resolution functions were tried. As an example we mention that the use of the rather high d-wave phase shift obtained by Dubé *et al.* [55] systematically lowered the fitted resonance width by about 0.3 meV.

For comparison with the present results, Table 2 lists earlier determinations of the resonance position E_r and the resonance width Γ. Within the respective uncertainties, our experimental and theoretical results for the resonance width are in very good agreement with the experimental value of Kennerly *et al.* [18] and with several theoretical results [67,69,74–77]. A width close to 9 meV, obtained in earlier experimental work including that of the Manchester group [90,94], must be considered as too low. The recent experimental value $\Gamma = 10.3(3)$ meV, obtained by Dubé *et al.* [55] from an analysis of the resonance line shapes at several angles between 50° and 130° (energy width between 30 and 50 meV), is also somewhat low.

Our experimental result for the resonance position is the most precise determination so far. The previously recommended value of 19.366(5) meV [5,94], determined relative to the onset for $He^*(2^3S_1)$ excitation (present as a downward cusp in the elastic scattering intensity), is in excellent agreement with our result. Figure 12 illustrates the historical evolution of the experimental and theoretical determinations of the width and the energy of the $He^-(1s\ 2s^2\ ^2S_{1/2})$ resonance.

5 Conclusions

A new experimental setup has been presented and characterized which combines a laser photoelectron source with a dense supersonic beam target in order to study elastic and inelastic electron scattering from atoms and molecules in the gas phase at very high resolution. As a first demonstration we have revisited the $He^-(1s\ 2s^2\ ^2S_{1/2})$ resonance at an effective experimental energy width around 7.5 meV. Based on an accurate calibration of the electron energy scale by simultaneously measuring the onset for the production of metastable $He^*(2^3S_1)$ atoms, the resonance energy is determined with unprecedented precision as $E_r = 19.365(1)$ eV. Our result for the resonance width ($\Gamma = 11.2(5)$ meV) is in excellent agreement with the previous experimental benchmark value [18] and with the result of the R-matrix with pseudo states (RMPS) calculation [45]. Efforts are being taken to further reduce the experimental energy width and to study other narrow resonances in atoms and molecules.

Table 2. Energy position E_r and natural width Γ of the $He^-(1s\ 2s^2\ ^2S_{1/2})$ resonance.

Reference	E_r [eV]	Γ [meV]	Label (Fig. 12)
Theory			
Burke *et al.* [60]	19.33		T1
Temkin *et al.* [65]	19.363	14.4	T2
	19.386	13.9	
Sinfailam and Nesbet [66]	19.4	15	T3
Ormonde and Golden [67]	19.38	11.5	T4
Wickmann and Heiss [68]		22	T5
Bain *et al.* [69]	19.398	12	T6
Berrington *et al.* [70]		15.3	T7
Barden *et al.* [71]		8.0	T8
Hata [72]		34	T9
Hata [73]	19.34(4)		T10
Junker [74]	19.387	11.72	T11
Hazi [75]	19.40	11.5	T12
Foster *et al.* [76]		11.0	T13
Burke *et al.* [77]		11.72	T14
Berk *et al.* [78]	19.504		T15
Bylicki [79]	19.367	8.6	T16
Thomasz *et al.* [80]	19.357	14	T17
this work	19.366	10.7	T18
Experiment			
Simpson and Fano [81]		10	E1
Ehrhardt *et al.* [83][a]		12	E2
Gibson and Dolder [84]		8	E3
Golden and Zecca [85]		8(2)	E4
Kisker [86]	19.33(2)		E5
Sanche and Schulz [87]	19.34(2)		E6
Preston *et al.* [88]		13(4)	E7
Golden *et al.* [89]		13	E8
Cvejanovic *et al.* [90]	19.367(9)	9(1)	E9
Cvejanovic and Read [91]	19.361(9)		E10
Huetz [92]	19.369(10)		E11
Roy *et al.* [93]		8 - 10	E12
Brunt *et al.* [56]	19.367(7)		E13
Brunt *et al.* [94]	19.366(5)	9(1)	E14
Kennerly *et al.* [18]	19.36(2)	11.0(5)	E15
Buckman *et al.* [57]	19.367(5)		E16
Dubé *et al.* [55]		10.3(3)	E17
this work	19.365(1)	11.2(5)	E18

[a] Resonance width quoted on page 186 of [83], replacing earlier estimate of 15–20 meV given by Andrick and Ehrhardt [82].

This work has been supported by the Deutsche Forschungsgemeinschaft (Ho 427/24 and Forschergruppe *Niederenergetische Elektronenstreuprozesse*) and by the Zentrum für Lasermesstechnik and Diagnostik. We gratefully acknowledge the mechanical workshop of Universität Kaiserslautern for their remarkable achievement in the realization of the new apparatus. We thank M. Allan and F. Linder for fruitful discussions of various aspects of low-energy electron scattering, E. Leber, J.M. Weber, S. Barsotti, and S. Marienfeld for experimental cooperation regarding the laser photoelectron source, and K. Zinsmeister for technical support. One of us (KB) acknowledges support by the United States National Science Foundation under grant PHY-0088917 and, in part, through a grant for the Institute of Theoretical Atomic and Molecular Physics at Harvard University and the Smithsonian Astrophysical Observatory.

References

1. G.J. Schulz, Rev. Mod. Phys. **45**, 378 (1973); *ibid.* 423
2. *Applied Atomic Collision Physics*, edited by H.S.W. Massey, D.R. Bates (Academic Press, New York, 1982), Vol. 1
3. *Electron-molecule collisions*, edited by I. Shimamura, K. Takayanagi (Plenum Press, New York, 1984)
4. *Electron-molecule interactions and their applications*, edited by L.G. Christophorou (Academic Press, New York, 1984), Vols. I and II
5. S.J. Buckman, C.W. Clark, Rev. Mod. Phys. **66**, 539 (1994)
6. A. Zecca, G.P. Karwasz, R.S. Brusa, Riv. Nuovo Cim. **19**, 1 (1995)
7. L.G. Christophorou, J.K. Olthoff, Adv. At. Mol. Opt. Phys. **44**, 59 (2000)
8. M.J. Brunger, S.J. Buckman, Phys. Rep. **357**, 215 (2002)
9. K.P. Rohr, F. Linder, J. Phys. B **9**, 2521 (1976)
10. K. Jung, Th. Antoni, R. Müller, K.H. Kochem, H. Ehrhardt, J. Phys. B **15**, 3535 (1982)
11. F.H. Read, Phys. Scripta **27**, 103 (1983)
12. M. Allan, J. Phys. B **28**, 5163 (1995)
13. M. Allan, Phys. Rev. Lett. **87**, 033201 (2001)
14. H. Ibach, J. Electron. Spectrosc. Relat. Phenom. **64/65**, 819 (1993)
15. H. Ibach, Surf. Sci. **299/300**, 116 (1994)
16. A.C. Gallagher, G. York, Rev. Sci. Instrum. **45**, 662 (1974)
17. R.J. van Brunt, A.C. Gallagher, in *Electronic and Atomic Collisions*, edited by G. Watel (North Holland, Amsterdam, 1978), p. 129
18. R.E. Kennerly, R.J. van Brunt, A. Gallagher, Phys. Rev. A **23**, 2430 (1981)
19. P. Hammond, J. Phys. B **29**, L231 (1996)
20. J. Comer, F.H. Read, J. Phys. B **4**, 1055 (1971)
21. J. M. Ajello, A. Chutjian, J. Chem. Phys. **71**, 1079 (1979)
22. A. Chutjian, S.H. Alajajian, Phys. Rev. A **31**, 2885 (1985)
23. A. Chutjian, A. Garscadden, J.M. Wadehra, Phys. Rep. **264**, 393 (1996)
24. D. Field, J.P. Ziesel, P.M. Guyon, T.R. Govers, J. Phys. B **17**, 4565 (1984)
25. D. Field, G. Mrotzek, D.W. Knight, S. Lunt, J.P. Ziesel, J. Phys. B **21**, 171 (1988)
26. D. Field, D.W. Knight, G. Mrotzek, J. Randell, S.L. Lunt, J.B. Ozenne, J.P. Ziesel, Meas. Sci. Technol. **2**, 757 (1991)
27. D. Field, N.C. Jones, J.M. Gingell, N.J. Mason, S.L. Lunt, J.P. Ziesel, J. Phys. B **33**, 1039 (2000)
28. D. Field, S.L. Lunt, J.P. Ziesel, Acc. Chem. Res. **34**, 291 (2001)
29. J.P. Ziesel, J. Randell, D. Field, S.L. Lunt, G. Mrotzek, P. Martin, J. Phys. B **26**, 527 (1993)
30. D. Klar, M.-W. Ruf, H. Hotop, Aust. J. Phys. **45**, 263 (1992)
31. D. Klar, M.-W. Ruf, H. Hotop, Meas. Sci. Technol. **5**, 1248 (1994)
32. A. Schramm, J.M. Weber, J. Kreil, D. Klar, M.-W. Ruf, H. Hotop, Phys. Rev. Lett. **81**, 778 (1998)
33. D. Klar, M.-W. Ruf, H. Hotop, Int. J. Mass Spectrom. **205**, 93 (2001)
34. M. Keil, T. Kolling, K. Bergmann, W. Meyer, Eur. Phys. J. D **7**, 55 (1999)
35. J.M. Weber, E. Leber, M.-W. Ruf, H. Hotop, Phys. Rev. Lett. **82**, 516 (1999)
36. J.M. Weber, M.-W. Ruf, H. Hotop, Eur. Phys. J. D **7**, 587 (1999)
37. I.D. Petrov, V.L. Sukhorukov, E. Leber, H. Hotop, Eur. Phys. J. D **10**, 53 (2000)
38. J. Bömmels, E. Leber, A. Gopalan, J.M. Weber, S. Barsotti, M.-W. Ruf, H. Hotop, Rev. Sci. Instrum. **72**, 4098 (2001)
39. R. Campargue, J. Phys. Chem. **88**, 4466 (1984)
40. S. Götte, A. Gopalan, J. Bömmels, M.-W. Ruf, H. Hotop, Rev. Sci. Instrum. **71**, 4070 (2000)
41. A. Gopalan, E. Leber, J. Bömmels, S.P.H. Paul, M. Allegrini, M.-W. Ruf, H. Hotop, Meas. Sci. Technol. (submitted)
42. E. Leber, S. Barsotti, I.I. Fabrikant, J.M. Weber, M.-W. Ruf, H. Hotop, Eur. Phys. J. D **12**, 125 (2000)
43. W.C. Martin, J. Phys. Chem. Ref. Data **2**, 257 (1973)
44. P.J. Mohr, B.N. Taylor, J. Phys. Chem. Ref. Data **28**, 1713 (1999)
45. K. Bartschat, E.T. Hudson, M.P. Scott, P.G. Burke, V.M. Burke, Phys. Rev. A **54**, R998 (1996)
46. K. Bartschat, J. Phys. B **31**, L469 (1998)
47. E.P. Wigner, Phys. Rev. **73**, 1002 (1948)
48. T. Miller, B. Bederson, Adv. At. Mol. Phys. **13**, 1 (1978)
49. P. Frey, M. Lawen, F. Breyer, H. Klar, H. Hotop, Z. Phys. A **304**, 155 (1982)
50. N.F. Mott, H.S.W. Massey, *The Theory of Atomic Collisions* (Oxford University Press, Oxford, 1965)
51. D. Andrick, A. Bitsch, J. Phys. B **8**, 393 (1975)
52. J.F. Williams, J. Phys. B **12**, 265 (1979)
53. R.K. Nesbet, Phys. Rev. A **20**, 58 (1979)
54. D.G. Thompson, Proc. Roy. Soc. Lond. A **294**, 160 (1966)
55. D. Dubé, D. Tremblay, D. Roy, Phys. Rev. A **47**, 2893 (1993)
56. J.N.H. Brunt, G.C. King, F.H. Read, J. Phys. B **10**, 433 (1977)
57. S.J. Buckman, P. Hammond, F.H. Read, G.C. King, J. Phys. B **16**, 4039 (1983)
58. W.L. Wiese, M.W. Smith, B.M. Glennon, *Atomic Transition Probabilities – Hydrogen through Neon* (NSRDS-NBS 4, 1966), Vol. 1
59. H. Hotop, in *Experimental Methods in the Physical Sciences, Atomic, Molecular, and Optical Physics: Atoms and Molecules*, edited by F.B. Dunning, R.G. Hulet (Academic Press, San Diego, 1996), Vol. 29B, p. 191
60. P.G. Burke, J.W. Cooper, S. Ormonde, Phys. Rev. **183**, 245 (1969)
61. R.S. Oberoi, R.K. Nesbet, Phys. Rev. A **8**, 2969 (1973)
62. R.K. Nesbet, Phys. Rev. A **12**, 444 (1975)
63. M. Allan, J. Phys. B **25**, 1559 (1992)
64. M. Allan, J. Phys. B **33**, L215 (2000)
65. A. Temkin, A.K. Bhatia, J.N. Bardsley, Phys. Rev. A **5**, 1663 (1972)
66. A.L. Sinfailam, R.K. Nesbet, Phys. Rev. A **6**, 2118 (1972)
67. S. Ormonde, D.E. Golden, Phys. Rev. Lett. **31**, 1161 (1973)
68. E. Wickmann, P. Heiss, J. Phys. B **7**, 1042 (1974)
69. R.A. Bain, J.N. Bardsley, B.R. Junker, C.V. Sukumar, J. Phys. B **7**, 2189 (1974)
70. K.A. Berrington, P.G. Burke, A.L. Sinfailam, J. Phys. B **8**, 1459 (1975)
71. I.R. Barden, C. Bottcher, K.R. Schneider, J. Phys. B **8**, L1 (1975)
72. J. Hata, Phys. Lett. A **55**, 19 (1975)

73. J. Hata, J. Chem. Phys. **66**, 1266 (1977)
74. B.R. Junker, Phys. Rev. A **18**, 2437 (1978)
75. A.U. Hazi, J. Phys. B **11**, L259 (1978)
76. G. Foster, D.G. Hummer, D.W. Norcross, Bull. Am. Phys. Soc. **24**, 1183 (1979)
77. P.G. Burke, L.C.G. Freitas, A.E. Kingston, K.A. Berrington, in "Electronic and Atomic Collisions", Abstracts of Contributed Papers, *XIIIth ICPEAC*, Berlin, 1983, edited by J. Eichler, W. Fritsch, I.V. Hertel, N. Stolterfoth, U. Wille (Berlin, 1983), p. 108
78. A. Berk, A.K. Bhatia, B.R. Junker, A. Temkin, Phys. Rev. A **34**, 4591 (1986)
79. M. Bylicki, J. Phys. B **23**, 413 (1991)
80. J.G. Thomasz, C.W. McCurdy, H.L. Byron, J. Phys. B **26**, 509 (1993)
81. J.A. Simpson, U. Fano, Phys. Rev. Lett. **11**, 158 (1963)
82. D. Andrick, H. Ehrhardt, Z. Phys. **192**, 99 (1966)
83. H. Ehrhardt, D. Andrick, F. Linder, Z. Phys. **214**, 179 (1968)
84. J.R. Gibson, K.T. Dolder, J. Phys. B **2**, 741 (1969)
85. D.E. Golden, A. Zecca, Rev. Sci. Instrum. **42**, 210 (1971)
86. E. Kisker, Z. Phys. **256**, 121 (1972)
87. L. Sanche, G.J. Schulz, Phys. Rev. A **5**, 1672 (1972)
88. J.A. Preston, M.A. Hender, J.W. McConkey, J. Phys. E **6**, 661 (1973)
89. D.E. Golden, F.D. Schowengerdt, J. Macek, J. Phys. B **7**, 478 (1974)
90. S. Cvejanovic, S. Comer, F.H. Read, J. Phys. B **7**, 468 (1974)
91. S. Cvejanovic, F.H. Read, J. Phys. B **7**, 1180 (1974)
92. A. Huetz, Ph.D. thesis, University of Paris, quotation from [94]
93. D. Roy, A. Delage, J.D. Carette, J. Phys. E **8**, 109 (1975)
94. J.N.H. Brunt, G.C. King, F.H. Read, J. Phys. B **10**, 1289 (1977)